Journal of Catalysis 327 (2015) 86–95

Contents lists available at ScienceDirect

Journal of Catalysis

journal homepage: www.elsevier.com/locate/jcat

Influence of the pretreatment conditions on the development and performance of active sites of Pt/TiO_2 catalysts used for the selective citral hydrogenation

Esther Bailón-García, Francisco Carrasco-Marín, Agustín F. Pérez-Cadenas, Francisco J. Maldonado-Hódar *

Department of Inorganic Chemistry, Faculty of Sciences, University of Granada, Avda. Fuentenueva s/n, 18071 Granada, Spain

ARTICLE INFO

Article history:
Received 11 March 2015
Revised 16 April 2015
Accepted 17 April 2015

Keywords:
Pt catalysts
TiO_2-support
Pretreatment conditions
Oxygen vacancies
Metal–support interactions
Unsaturated alcohols

ABSTRACT

The influence of pretreatment conditions of Pt/TiO_2 catalysts was analyzed by different techniques and changes in the textural and chemical properties correlated with the catalytic performance in citral hydrogenation. After H_2 pretreatment, the formation of two-dimensional Pt nanoparticles and oxygen vacancies favors the diffusion of Pt species into the TiO_2 structure, while three-dimensional Pt crystallites are formed after He pretreatment. The coupled effect of Pt 2-D nanoparticles and oxygen vacancies strongly enhances the catalytic activity and the selective hydrogenation of citral to unsaturated alcohols by favoring the citral adsorption on the reduced surface through the terminal C=O groups in an environment rich in hydrogen provided by the highly dispersed Pt nanoparticles. These coupled metal-vacancy active sites are formed also after a combined He/H_2 pretreatment; nevertheless, the formation of three-dimensional Pt particles during the previous He treatment strongly reduce the extent of TiO_2–Pt interface and consequently the surface site concentration and the catalytic activity.

1. Introduction

Citral (3,7-dimethyl-2,6-octadienal) is an isomeric mixture of the acyclic aldehydes geranial (citral E) and neral (citral Z). The demand of their derivatives unsaturated alcohols (UA), geraniol and nerol by chemical, pharmaceutical or perfumery industries, progressively increases. Citral is found in plants and citrus fruits but very recently came to be produced petrochemically in very large quantities [1]. Although geraniol can be isolated from palmarosa oil and nerol was obtained from the oil of nerol [2,3], the selective hydrogenation of citral is one of the more feasible ways for obtaining these unsaturated alcohols at large scale.

Nevertheless, in the selective hydrogenation of α,β-unsaturated aldehydes, thermodynamic and kinetic factors favor the hydrogenation of the conjugated C=C over the C=O bond [4], and thus, the saturated aldehyde or alcohol is mainly obtained. In addition, secondary reactions of hydrogenation, isomerization, cyclization, or cracking also take place leading to a complex reaction pathway [5]. The challenge is to selectively enhance the hydrogenation of the C=O bond to UA, which can only be achieved with an optimal design of the catalyst. Different approaches for this objective were previously published, by studying the influence of supports [6–8], active phases [9,10], and the interactions between them [6,11,12].

The nature and effect of the strong metal–support interactions (SMSI) were early shown by Tauster and Fung [13] and related with the support reducibility. Nevertheless, SMSI is even today a matter of discussion and generates a field of great research interest in the development of selective hydrogenation catalysts. In this sense, recently the influence of impregnation procedures and pretreatments at different temperatures (300 vs 500 °C) in H_2 flow of Pt/TiO_2 and Rh/TiO_2 catalysts used in the citral hydrogenation was described [14]. It is suggested that with increasing temperature, conversion decreases but selectivity to UA increases as consequence of the formation of TiO_{2-X} species (no identified), because these effects were not observed using the same active phases on non-reducible Al_2O_3 as support [15]. It was also suggested [16] that the improved hydrogenation performance of Pt catalysts using TiO_2/SiO_2 composite as support regarding pure TiO_2 is due to a stronger SMSI effect in the first case, because the formation of anatase nanocrystallites facilitates the interactions with Pt after reduction.

These works are focused mainly on catalytic results, but there is a lack of information about the chemical and structural modifications caused by pretreatments, the identification of Pt species on reduced TiO_2 surfaces, and the influence of such species on the catalytic performance. In this manuscript, we analyze by different

* Corresponding author. Fax: +34 958248526.
E-mail address: fjmaldon@ugr.es (F.J. Maldonado-Hódar).

http://dx.doi.org/10.1016/j.jcat.2015.04.019
0021-9517/

techniques Pt/TiO_2 catalysts before and after pretreatments in different experimental conditions. The structural and chemical changes detected are related with the catalytic performance obtained.

2. Experimental

2.1. Catalysts preparation

Commercial TiO_2 (anatase, Alfa Aesar) without additional treatments was milled and sieved to a diameter smaller than 0.150 mm before impregnation. Platinum catalysts were prepared by impregnation at 3 wt% Pt loading using an aqueous solution containing the appropriate amount of $[Pt(NH_3)_4]Cl_2$, dried, and finally pretreated in He or H_2 flow at 400 °C (heating rate of 5 °C/min) for 12 h. An alternative pretreatment where the precursor salt is decomposed initially for 2 h at 400 °C in He and after that treated in H_2 flow for additional 10 h was also carried out. Catalysts were referred indicating the reduction treatment. Thus, as an example, Pt/TiO_2-He indicates that Pt was deposited on TiO_2 support and pretreated in He flow.

2.2. Textural and chemical characterization

Textural characterization was carried out by N_2 adsorption at −196 °C using a Quantachrome Autosorb-1 equipment. The BET equation was applied to the N_2 adsorption isotherms to determine the apparent surface area (S_{BET}), and the Dubinin–Radushkevich and Stoeckli equations were used [17–20] to determine the micropore volume (W_0) and the mean micropore width (L_0). The total pore volume (V_{Total}) was considered [21] as the volume of N_2 adsorbed at $P/P_0 = 0.95$ and the mesopore volume (V_{meso}) consequently calculated by difference.

Pt dispersion (D) and mean particle size (d) were obtained by X-ray diffraction (XRD), H_2 chemisorption, and high-resolution transmission electron microscopy (HRTEM). Chemisorption isotherms were measured in conventional volumetric equipment. Equilibrium pressure was measured with a precision of 0.1 mbar. 0.250 g of the supported catalyst was pretreated as described above and outgassed at 350 °C for 1 h. Subsequently, it was cooled down to 25 °C and a H_2 adsorption isotherm was measured between 70 and 350 mbar. H_2 uptake was determined from the intercept of the linear adsorption isotherm. Platinum dispersion, D, namely the ratio between surface (M_S) and total metal atoms (M_T), and the average Pt particle size, $\bar{d}(\text{nm}) = \frac{1.08}{D}$, were obtained from the H_2 uptake assuming, respectively, a stoichiometric ratio H_2:Pt = 1:2 (dissociative chemisorption) and the formation of spherical particles [22,23].

HRTEM images were recorded using a FEI TITAN G2 80-300 microscope equipped with a scanning transmission electron microscopy (STEM) detector-type HAADF (high-angle annular dark-field detector), corrector of spherical aberration (CEOS), and EDX microanalysis system (Super X). This equipment has a maximum resolution of 0.8 Å (TEM) or 1.4 Å (STEM), working with an acceleration voltage of 300 kV. A small amount of well-milled catalysts is dispersed in ethanol under ultrasound and mounted on a 300 mesh carbon-coated cooper grid. Always more than 100 Pt particles were analyzed by the appropriate software in order to obtain the particle size distributions and the average particle size.

X-ray diffraction (XRD) pattern were recorded using a Bruker D8 Advance X-ray diffractometer with Cu Kα radiation. The 2θ angles were scanned from 10 to 90°. The average Pt crystallite sizes (D) were estimated by the application of the Debye–Scherer formula, $D = 0.95\lambda/\beta\cos\theta$ to the {1 1 1} peak of platinum, where θ is the diffraction angle and β is the full width at half-maximum (fwhm). The fwhm was determined with an extrapolated baseline between the beginning (low angle side) and the end (high-angle side) of a diffraction peak with the highest intensity.

The chemical characterization of the catalysts was further analyzed by X-ray photoelectron spectroscopy (XPS). The spectra were obtained on a Kratos Axis Ultra-DLD X-ray photoelectron spectrometer equipped with a hemispherical electron analyzer connected to a detector DLD (delay-line detector). For these measurements, the binding energy (BE) values were referred to the C_{1s} peak at 284.6 eV, and the Pt_{4f}, O_{1s}, and Ti_{2p} spectral regions were scanned several times to obtain good signal-to-noise ratios. The spectra obtained after background signal correction were fitted to Lorentzian and Gaussian curves in order to obtain the number of components, the position of each peak, and the peak areas. Finally, all the components were assigned according to the bibliography [24–27].

Information about the support acidity was obtained by measuring the pH_{pzc}, according to the methodology previously described [28], and the strength and amount of acid sites of pretreated catalyst were studied by n-butylamine adsorption/desorption (TPD) experiments. Dynamic adsorption/desorption tests (TPD) were carried out in a quartz microreactor at atmospheric pressure with 0.2 g of sample using a He/Ar flow (total flow rate 60 $cm^3\ min^{-1}$) saturated with n-butylamine at 0 °C (partial pressure of n-butylamine 28.92 Torr). Analyses were carried out online with a Mass Spectometer model Prisma (Pfeiffer). Samples were heated in pure He flow up to the adsorption temperature (150 °C), and after stabilization, the He flow was turned by the saturated He/Ar flow up to sample saturation (the n-butylamine concentration is recovered). After that, the saturated sample was purged in pure He for 1 h to remove rest of trapped n-butylamine, and then, TPD-n-butylamine was recorded by heating at 10 °C/min.

2.3. Catalytic performance

The citral hydrogenation was carried out in 100 ml heptane solution at a constant hydrogen pressure of 8.3 bar and 90 °C using a Parr reactor model 5500. The experimental conditions, citral concentration, catalyst weight, and agitation speed, were previously optimized in order to avoid mass transfer limitations (results not shown) and fixed in 0.05 M, 500 mg, and 1500 rpm, respectively. A small volume of sample (1 mL) was periodically withdrawn and analyzed by chromatography using a Bruker 430-GC equipped with a FID detector and a Varian GC Capillary Column CP7485 (25 m × 0.32 mm × 0.45 μm). Citral and any possible product were previously calibrated.

3. Results and discussion

The catalytic performance after reduction of Pt/TiO_2 in pure He or H_2 flow, and the combined reduction cycle (He/H_2), is compared in Fig. 1. Clearly, both activity and selectivity are strongly favored after H_2 pretreatment, in such a manner that total conversion is achieved after 6 h of reaction with unusual high values of selectivity to UA (S_{UA}, at around 80%) for monometallic Pt catalysts, which normally do not exceed S_{UA} values of 50–55% [5]. Selectivity values only decay at conversions greater than 80%, where secondary hydrogenations are favored. On the contrary, the smallest activity and selectivity values are detected after pretreatment in He flow. Moreover, in this case, S_{UA} decreases even at significantly low conversion values (Fig. 1), indicating that secondary reactions are favored. In the case of the combined He/H_2 pretreatment, while the catalytic activity is similar to the obtained after the He pretreatment, the selectivity values are quite similar those obtained after H_2 pretreatment. This combined pretreatment point out that,

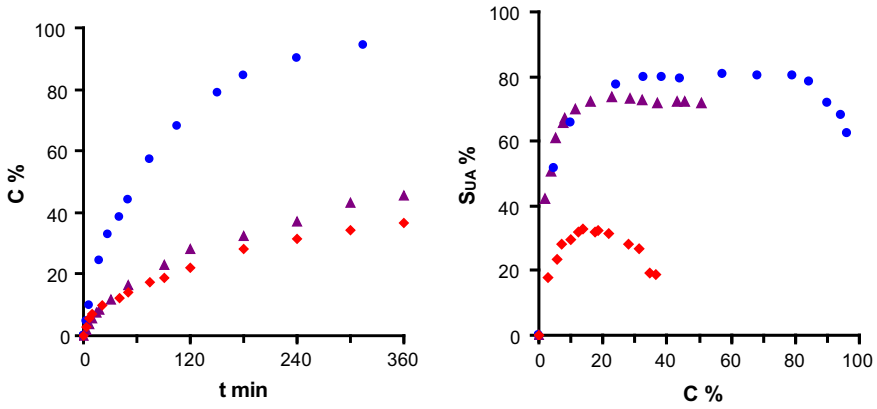

Fig. 1. Influence of pretreatment conditions on the catalytic performance of Pt/TiO_2 catalysts (a) Evolution of the conversion with reaction time (b) selectivity to unsaturated alcohols with increasing conversion values. Pt/TiO_2–He (◆), Pt/TiO_2–H_2 (●), and Pt/TiO_2–He, H_2 (▲).

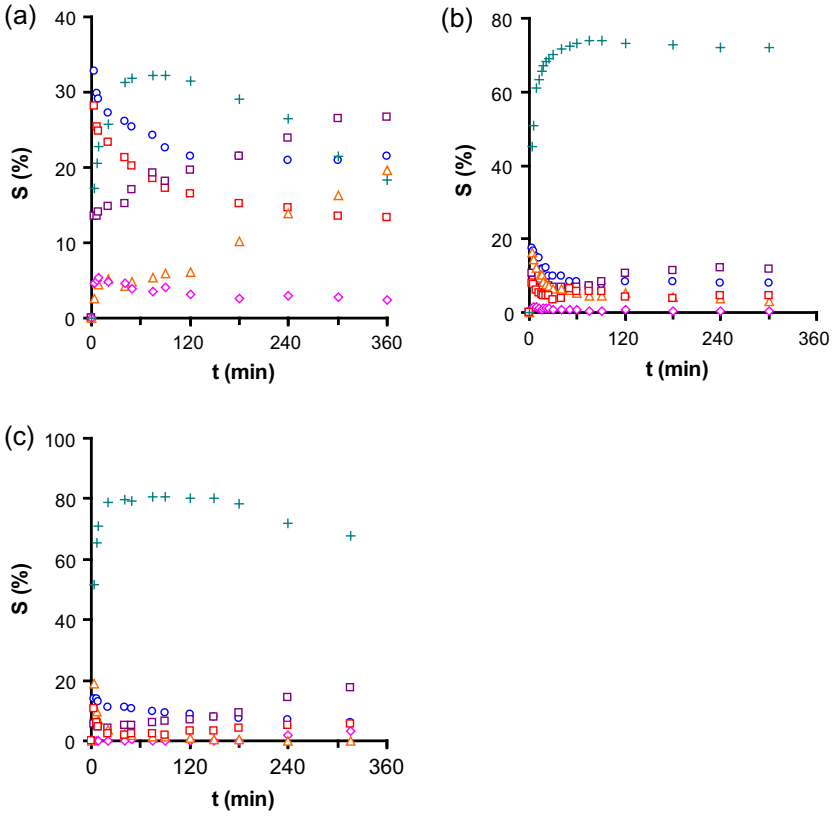

Fig. 2. Products distribution along the reaction development: (a) Pt/TiO_2–He, (b) Pt/TiO_2–He, H_2, and (c) Pt/TiO_2–H_2. Citronellal (○), S_{UA} (+), Cyclization = isopulegol + menthol (△), citronellol (□), 3, 7 DMO (◇), cracking (□). Reaction conditions: citral in heptane solution (0.05 M), 500 mg of catalyst, 1500 rpm, 90 °C, and PH_2 = 8.3 bar.

while the number of active sites (activity) is determined by the previous He pretreatment, the nature of the selective hydrogenation sites is determined by the H_2 pretreatment. This means that H_2 pretreatment generates some transformations that activate specifically the catalyst surface favoring the hydrogenation of citral to UA.

It is noteworthy that S_{UA} initially increases independently of the pretreatment used (Fig. 1b); this means that there is always an induction period where the active sites are progressively accommodated to the reaction development. This fact can be related with the total product distribution obtained in each case (Fig. 2). Thus, it is observed that after He pretreatment, initially the stronger active sites produce the preferential hydrogenation of C=C bonds (to citronellal) and cracking of the citral molecules, but these sites are progressively deactivated. Cracking reactions are induced by the support acidity [29]. Simultaneously, citronellal is transformed by secondary hydrogenation or cyclization reactions to citronellol or menthol and isopulegol, respectively. After 2 h of reaction, also the S_{UA} decreases because they are also transformed into citronellol. However, after H_2 pretreatment, UA are always the main reaction product obtained, denoting the different nature of the active sites and the different interaction of the catalyst surface with the citral molecules that in this case are hydrogenated through the C=O bonds. The increase of S_{UA} during the induction

period is also due to the deactivation of the C=C hydrogenation sites, while cracking is significantly reduced, because this pretreatment also leads to an acidity decrease, as shown below. After that, the product distribution becomes very stable and only citronellol slowly increases at high conversion values by hydrogenation of UA. However, it is noteworthy that these secondary processes develop in a smaller proportion than in the previous case, denoting the weak interaction of the C=C bonds with these active sites. The products distribution obtained after He/H_2 pretreatment is quite similar to that obtained after H_2 pretreatment, in spite of that the catalytic activity is considerably smaller. Thus, as commented, the nature of active sites seems to be similar, but they are present in a smaller proportion.

Different factors can influence this catalytic behavior; thus, textural properties and acidity of catalysts, and Pt nature and dispersion, were carefully analyzed. Textural parameters can influence the citral adsorption mode and/or the adsorption capacity. In a previous paper [30], it was suggested that in order to increase the selectivity toward unsaturated alcohols, geometrical effects derived from the zeolite pore size and shape and location of ruthenium particles in the KL structure are more effective than the electronic modifications induced by electron-donor supports. Textural parameters obtained from the analysis of the N_2 adsorption isotherms are summarized in Table 1. The BET surface area of pretreated catalysts are quite similar to the BET surface of the support, but the total pore volume ($V_{0.95}$) slightly decreases by certain porous blockage caused by the Pt nanoparticles loaded. This blockage takes place mainly in the mesopore range (V_{meso} decreased) where Pt nanoparticles should be located although also leads to narrowest micropores (L_0). Nevertheless, the textural parameters determined for pretreated catalysts show similar values between them, and therefore, the variations of the catalytic behavior seem not to be due to textural changes after the different pretreatments. Moreover, the mesoporous character of the support avoids the development of steric restriction that could favor a preferential adsorption mode.

The catalytic performance is also related with the catalysts acidity and the strength of the acid sites. We have pointed out that the strong Brönsted acidity of Al_2O_3 favors the activity at the expense of a very high cracking selectivity regarding other inorganic supports [29,31]. However, recently it was also found that basic catalysts are more active and more selective to citronellal, while acid sites favor the formation of UA [32].

To analyze the influence of Pt precursor decomposition conditions on the acidity of the samples, both TiO_2 support and impregnated catalysts were pretreated in identical conditions. The pH_{pzc} of TiO_2 pretreated in He flow remain practically constant regarding the untreated sample (Table 2), but this parameter increases significantly after pretreatment in H_2 showing the release of some acid sites. This effect is similar for samples pretreated under consecutive He/H_2 flows. Pretreated catalysts are stronger acid materials than their supports pretreated in identical experimental conditions, indicating that Pt loading generate new acid sites. This behavior was previously observed by others authors [33]. Moreover, pretreatment atmosphere also influences the precursor decomposition and sintering [34]. Because in this study only TiO_2 is used as support and $[Pt(NH_3)_4]Cl_2$ as metal precursor, changes on the catalyst acidity only depend on the pretreatment conditions. The acidity of materials therefore is favored by the presence of Pt and decreases in all cases after H_2 pretreatments.

Table 1
Textural parameters of pretreated Pt/TiO_2 catalysts obtained from N_2 adsorption isotherms.

Catalyst	S_{BET}	W_0	L_0	V_{meso}	$V_{0.95}$
	$m^2\ g^{-1}$	$cm^3\ g^{-1}$	nm	$cm^3\ g^{-1}$	
TiO_2	116	0.047	1.89	0.446	0.493
Pt/TiO_2–He	115	0.040	1.65	0.397	0.437
Pt/TiO_2–He/H_2	94	0.032	1.64	0.412	0.444
Pt/TiO_2–H_2	111	0.045	1.62	0.397	0.442

S_{BET}: BET surface area, W_0: micropore volume, L_0: micropore width.
V_{meso}: mesopore volume and $V_{0.95}$: total pore volume.

Table 2
Values of the pH_{pzc} of pretreated supports and catalysts.

Pretreatment	TiO_2 support	Pt/TiO_2 catalyst
None	4.90	–
400 °C 12 h He	4.87	2.44
400 °C 2 h He, 10 h H_2	6.48	3.92
400 °C 12 h H_2	6.36	3.62

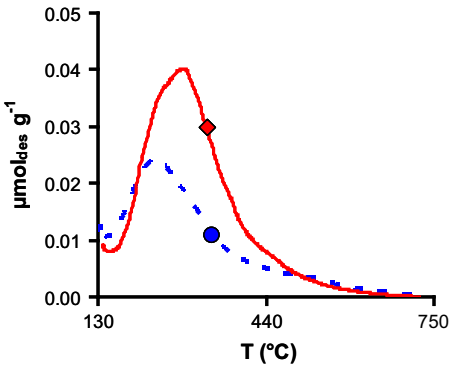

Fig. 3. TPD of n-butylamine after saturation at 150 °C. (●) Pt/TiO_2–H_2 (♦) Pt/TiO_2–He.

Results obtained from TPD of n-butylamine provide similar conclusions (Fig. 3). In this experimental conditions (after saturation at 150 °C to avoid physical adsorption of n-butylamine), it is observed that He pretreated catalyst presents a higher acidity and a greater number of acid sites in all the temperature range (in all the range of acid strength), but moreover, the position of the maximum shifted to lower desorption temperatures after pretreatment in H_2 (to weaker acid sites) which is also in agreement to conclusions obtained from pH_{pzc} measurements. The smaller acidity after H_2 pretreatment should favor the formation of citronellal [32]. However, this acidity decrease seem to influence strongly the evolution of the product distribution previously shown in Fig. 2a regarding 2b and c, avoiding in a large extent the formation of cracking products and the C=C hydrogenation; thus, we obtained the most selective catalyst to UA in these conditions.

The chemical characteristics of the catalysts surface were analyzed also by XPS. Some of the results obtained for TiO_2 and Pt characterization are summarized in Tables 3 and 4, respectively. Regarding TiO_2 (Table 3), the deconvolution of the Ti_{2p} spectral region of untreated and He pretreated samples only shows a component at binding energy BE = 459.5 eV, corresponding to Ti^{4+} species, while two components, at 530.8 and 532.5 eV, were used to fit the O_{1s} spectral region. The major component of O_{1s} spectral region corresponds to the 'bulk' oxygen atom in the stoichiometric TiO_2 form, while the high BE component could correspond to various oxygen-containing surface functional groups [25]. Mainly hydroxyl (—OH) or bridge surface oxygen (Ti—O—Ti) groups were described [27]. It is noteworthy that in spite of the surface oxygen content is maintained after the He pretreatment regarding untreated support (Table 3), the component at high BE significantly decreases regarding the untreated catalysts, which is consistent with the hydroxyl removal from TiO_2 by heating [26]. However, after the H_2

pretreatment, the oxygen content of support significantly decreases (around 25% of the initial value) and simultaneously, new components are needed to fit both the O_{1s} and Ti_{2p} spectral regions (Table 3 and Fig. 4). In both cases, BE is shifted to lower values indicating an electronic enrichment (reduction). The Ti_{2p} component at 457.9 eV and 456.5 eV were assigned to the presence of Ti^{3+} and even Ti^{2+} species, respectively (Fig. 4), in agreement to the BE values previously published [24]. These results are also in agreement with the release of acid sites previously described and the formation of oxygen vacancies. This fact was pointed out also by different authors using the FTIR analysis [35,36].

The XPS analysis also shows the chemical state and surface concentration of Pt species. The results from the analysis of the Pt_{4f} spectral region are shown in Table 4. Before pretreatment, the Pt concentration determined is greater than the total Pt loading (3% wt), showing a preferential localization of Pt particles on TiO_2 external surface. In this case, only Pt^{2+} is detected, indicating that there is not auto-reduction of the precursor salt during impregnation. On the contrary, a similar mixture of Pt^0 and Pt^{2+} was detected after any catalyst pretreatment. This fact can be due to the reoxidation of Pt species during storage, but also can indicate that pretreatments are not strong enough to guarantee the total precursor reduction. After pretreatments, Pt content (Pt_{XPS}) significantly decreases (around 50%) which can be related with Pt sintering. Sintering seems to be slightly favored by H_2 pretreatment, also in agreement with previous observations [34]. It is however noteworthy that the BE of both Pt^0 and Pt^{2+} species after H_2 pretreatment appeared at BE around 0.5 eV higher than in the case of He pretreated samples, therefore showing the contrary behavior described for Ti and O species. This behavior probably indicates some electronic transfer from Pt particles to the support (a smaller electron density on the Pt particles).

Table 3
Influence of pretreatments on the surface oxygen content, binding energy, and percentage of the components used to fit the XPS Ti_{2p} and O_{1s} spectral regions of Pt/TiO_2 catalysts.

Catalyst	BE (eV) Ti_{2p}	Peak %	BE (eV) O_{1s}	Peak %	% O_{xps}
Pt/TiO_2	459.5	100	530.8	80	40.33
			532.5	20	
Pt/TiO_2–He	459.5	100	530.8	92	41.02
			532.2	8	
Pt/TiO_2–H_2	456.5	9	527.9	15	30.02
	457.9	21	529.3	21	
	459.2	69	530.7	57	
			532.2	7	

Table 4
Pt surface concentration and distribution of Pt species determined by XPS.

Catalyst	BE (eV) Pt^0	Pt (0)%	BE (eV) Pt^{2+}	Pt (II)%	Pt/Ti*	$Pt_{XPS\%}$ Wt
Pt/TiO_2	–	–	72.9	100	0.019	4.2
Pt/TiO_2–He	70.9	68	71.5	32	0.007	2.0
Pt/TiO_2–H_2	71.5	73	72.0	27	0.007	1.9

* Pt/Ti atomic ratio; Pt_{xps} = surface Pt concentration.

Because no additional diffraction peaks were detected, these results indicate smaller and/or no crystalline Pt particles. This fact must influence the catalytic performance shown in Fig. 1.

This behavior was also pointed out by HRTEM. The high resolution images obtained (Fig. 6) permit to describe significant

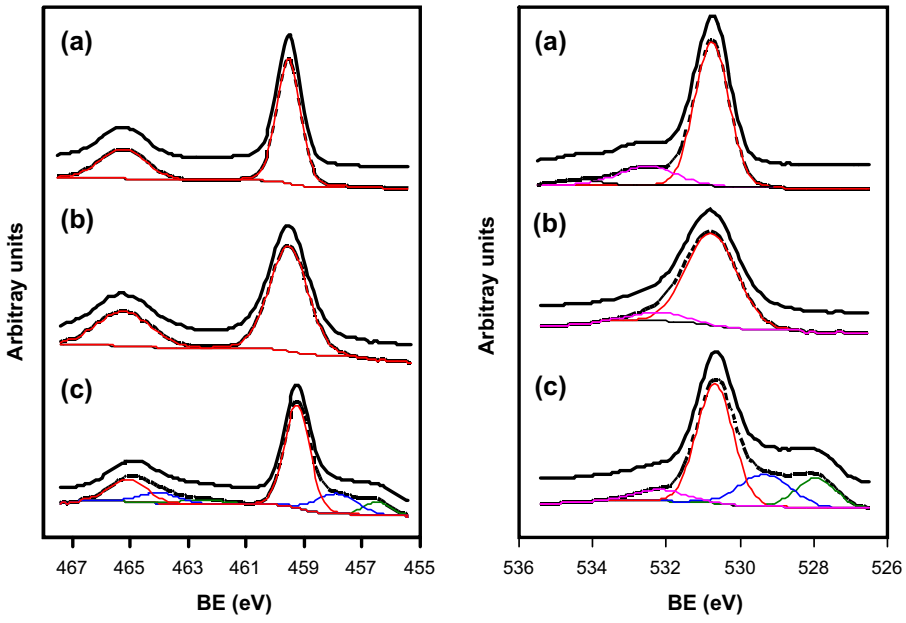

Fig. 4. Survey and deconvolution of the XPS Ti_{2p} (left) and O_{1s} (right) spectral regions (a) un-pretreated catalyst (Pt/TiO_2), (b) He pretreated catalyst (Pt/TiO_2–He), and (c) H_2 pretreated catalyst (Pt/TiO_2–H_2).

structural differences after the corresponding treatments. This technique confirms a higher Pt dispersion (smaller Pt particle size) after reduction in pure H_2. In this case, very small Pt nanoparticles of around 2 nm were detected, while after reduction in He or even He/H_2 cycle, large Pt particles, reaching some tens of nm are detected. Moreover, it is also noteworthy how the small Pt nanoparticles obtained after H_2 pretreatments seem to be eminently two-dimensional particles, i.e., Pt is mainly coating the TiO_2 surface forming thin films in such a manner that the TiO_2 crystallographic layers remain visible and clearly differentiated from the Pt ones (Fig. 6). The formation of this type of 2-D raft Pt particles were

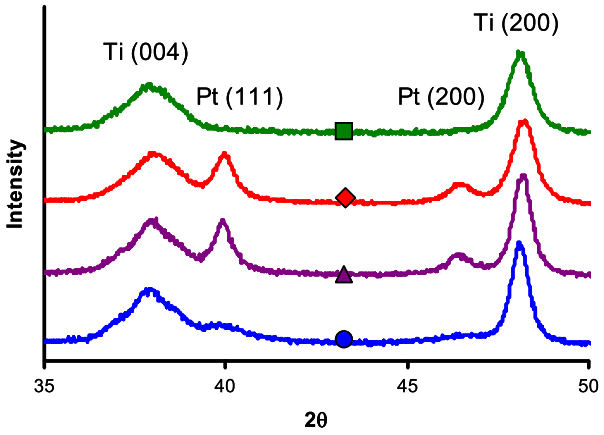

Fig. 5. XRD patterns of TiO_2 support and pretreated Pt/TiO_2 catalysts. TiO_2 (■), Pt/TiO_2–He (◆), Pt/TiO_2–He, H_2 (▲), and Pt/TiO_2–H_2 (●).

previously detected on different supports [39,40]. There is nevertheless a miss orientation between the crystallographic planes of TiO_2 support and Pt nanoparticles generating a high degree of imperfections and vacancies mainly in the surrounding interface area. Different regions (tentatively marked in red in Fig. 6b) were also observed on the TiO_2 particles showing different orientation as corresponding to polycrystalline substances. Measurements of the interlayer distance in Pt particles showed that the observed planes correspond to the $d_{hkl}(1\,1\,1) = 2.26$ Å.

It is well known that the citral hydrogenation is a structure sensitive reaction, strongly dependent on the Pt particle size [41–43]. Thus, we use complementary techniques previously discussed (XRD, H_2 chemisorption, and TEM) to determine the evolution of this parameter as described in the experimental section. Results are summarized in Table 5.

The average Pt nanoparticle size determined by H_2 chemisorption is very similar after any pretreatment, thus, although slightly increase in the case of H_2-pretreatment, Pt particle size only varies from 6.8 to 9.2 nm. The combined He/H_2 reduction cycle presents an intermediate behavior. This behavior is in agreement with the

Table 5
Amount of H_2 chemisorbed (Q_{H_2}) and average particle size ($\bar{d}$) determined by XRD, TEM, or H_2 chemisorption.

Catalyst	Q_{H_2}	$\bar{d}$XRD	$\bar{d}$TEM	$\bar{d}_{H_2}$
	μmol/g	nm		
Pt/TiO_2–He	12.1	10.6	9.1	6.8
Pt/TiO_2–He–H_2	11.7	12.6	11.6	7.7
Pt/TiO_2–H_2	9.0	–	3.6	9.2

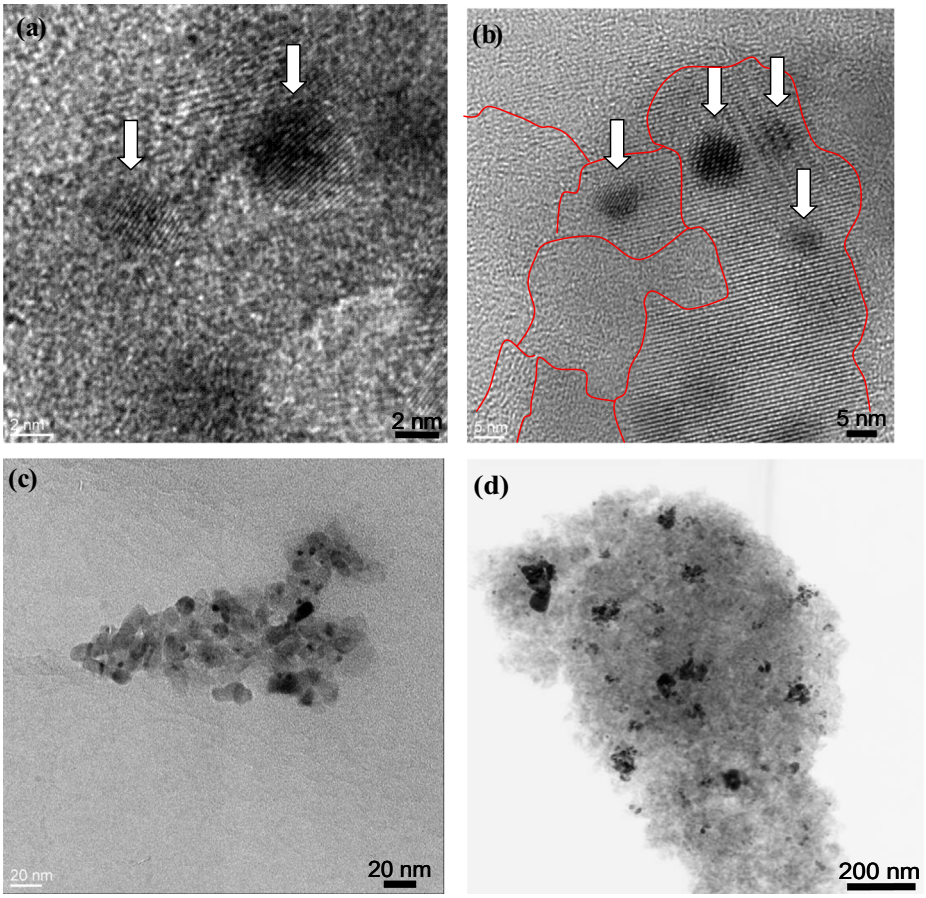

Fig. 6. HRTEM images of Pt/TiO_2 catalyst; (a and b) after H_2 pretreatment; Pt particles marked with an arrow (c) after He pretreatment (d) after He/H_2 pretreatment.

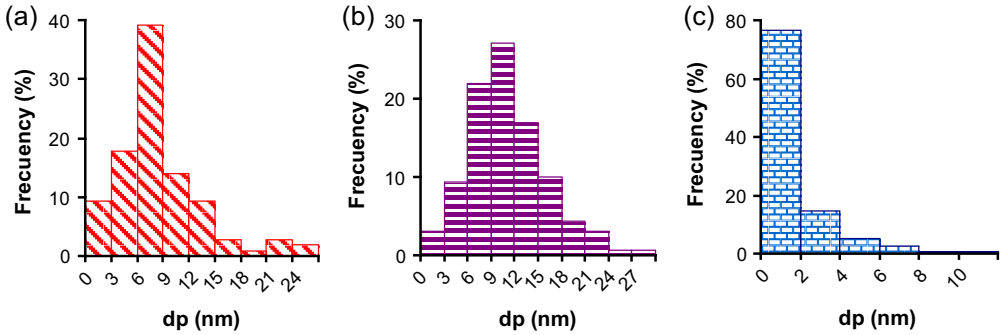

Fig. 7. Pt particle size distribution obtained by analysis of the HRTEM micrographs of pretreated catalysts: Pt/TiO_2–He (a) Pt/TiO_2–He/H_2 (b), and Pt/TiO_2–H_2 (c).

XPS results previously discussed. A good agreement among the average particle size values determined by the different techniques is also observed when catalysts are pretreated in He or He/H_2 flow. However, in the case of H_2 pretreated catalysts there is a great difference between the values determined by TEM and XRD, both indicating a high Pt dispersion (XRD showed very low intensity to be used, but this can be due to a small particle size) and H_2 chemisorption or XPS (both indicating a stronger sintering after H_2 pretreatment). Moreover, while H_2 chemisorption provides the higher values of the series, TEM provides the smaller ones. In Fig. 7 are compared the Pt particle size distribution obtained in each case.

Taking into account the characteristics of each technique, they can provide average Pt size values significantly different. Thus, XRD tend to provide an overestimated value, related mainly to the big crystalline particles while the smaller ones cannot be detected. On the contrary, in the case of H_2 chemisorption the amount adsorbed is greater on well dispersed catalysts, favoring consequently the determination of the smaller particles. H_2 chemisorption calculations [$d_{H2} = 1.08/D$ (nm)] also assume the spherical shape of particles. In the case of flat particles, dispersion (D) tends to unity as decrease the particle height, increasing progressively the area/volume ratio until the formation of a monolayer. In this sense, the particle size determined for H_2 pretreated catalysts by applying this equation progressively underestimates the mean particle size (even thus provide very high values). However, the different values obtained is not based on the error induced by this assumption, because really the amount of chemisorbed H_2 (Table 5, Q_{H2}) is smaller than after He pretreatment, i.e., there is a smaller amount of surface Pt atoms after H_2 pretreatment in spite the flat shape and the smaller size of these particles.

Due to the different mobility of the Pt-species during He or H_2 pretreatment [34] different structures can be formed. The mobility of metallic atoms (Pt, Rh, Ni) showing SMSI effects on defective titanium oxide lattices was previously described [24]. The role of H_2 in the mobilization of the metallic active phase was associated to the incorporation of hydrogen into oxygen vacancies at the reduced support, forming hydride-like species [i.e., $(Ti\text{-}H)^{3+}$] that may be responsible for the enhancement of the Pt mobility [44,45]. Thus, a different behavior is expected under He and H_2 pretreatment.

In our case, after He pretreatment the formation of 3D crystalline Pt particles was pointed out unequivocally by XRD and TEM, and results are in agreement with the average Pt particle size obtained by H_2 chemisorption. Only small and flat Pt nanoparticles are obtained after H_2 pretreatment, as observed by HRTEM, this morphology does not produce XRD peaks, but contrary to the expected, the H_2 uptake (surface Pt atoms) decrease even regarding large 3-D Pt particles, also in accordance with the Pt content detected by XPS. The key is therefore to find a suitable explanation for this fact taking into account that crystalline Pt particles are not formed. In these experimental conditions, the support reduction and the formation of oxygen vacancies were also unequivocally pointed out by XPS. Taking into account all these results, Pt^{2+} species should diffuse into the TiO_2 structure in agreement with the SMSI model proposed by Sanchez et al. [46] for reducible oxides. They describe the SMSI effects in terms of a "burial" of metallic particles that diffuse through the defective metal oxide lattice filling with metal atoms the oxygen vacancies favored by the hydrogen spillover and with elimination of oxygen of the anionic sub-lattice around them. The diffusion of Pt atoms through the oxygen vacancies of the TiO_2 structure, favored, as commented, by hydride-like species, provoke smaller Pt concentration and H_2 uptake values than those expected according to the Pt loading and Pt particle size observed by HRTEM. Recently, Ekou et al. [14] proposed that defective TiO_{2-X} moieties migrate and decorate the three-dimensional Rh or Pt particles. However, they found the contrary behavior, that is, the migration of metallic species into the supports. If the loss of H_2 uptake was due to Pt sintering and mobile TiO_{2-x} moieties decorating the Pt crystals, as proposed by Ekou et al. [14], XRD peaks of the Pt phase should be detected also in this case.

Correlating all the characterization results with the catalytic performance shown in Fig. 1 it is clear that the formation of the active sites, selective to the UA formation, needs the presence of H_2 during pretreatment to produce a synergetic effect between the reduced TiO_2 support and the Pt nanoparticle. It is clear that the metallic Pt nanoparticles generated after He pretreatment, are less selective without the cooperation of oxygen vacancies on the support. Thus, similar S_{UA} is obtained after He/H_2 and H_2 pretreatment (Fig. 1), due to the similar nature of the active sites generated. However, the catalytic activity is clearly smaller in the first case, which is related with a smaller active site concentration by formation of 3D Pt nanocrystals. When $[Pt(NH_3)_4]Cl_2$ precursor is previously decomposed in He flow the amount of active sites generated is strongly limited (and consequently the catalytic activity), because in this case the absence of oxygen vacancies constrain the mobility of Pt species that can move only on the support surface favoring sintering processes. An ulterior H_2 pretreatment strongly modify the Pt–support interactions and generates oxygen vacancies on the support (as shown by XPS) that enhance the citral adsorption through the C=O group and the consequently hydrogenation to UA. However, the greater Pt sintering leads to smaller support/Pt crystallite interphase. The higher activity and selectivity obtained after H_2 pretreatment is due to a better Pt dispersion and support reduction, very small Pt particles surrounded by a high concentration of oxygen vacancies. This pretreatment also produce an acidity decrease, avoiding in a large extent the development of cracking reactions, which also favors the S_{UA} increase regarding the He pretreatment.

The proposed reaction mechanism is tentatively summarized in Fig. 8. The adsorption and dissociation of H_2 molecules will be produced on the Pt particles, being this process favored by a decrease of the Pt particle size. The question is therefore to determine where and how are adsorbed the citral molecules in order to favor the catalytic activity and/or the S_{UA}. According to the bibliography, the preferential citral adsorption through the terminal C=O bond is induced by electrostatic interactions with the catalyst surface. Thus, doping with electropositive elements (Sn, Ga, In, etc) typically produces a S_{UA} increase by generating positive dipoles (δ^+) [47,48]. Nevertheless, it was also proposed that adsorption occurs on different sites depending on the chemical nature and structure of the reactant. Thus, Manyar et al. [49], using Pt-supported MnO octahedral molecular sieve (Pt/OMS-2 catalyst) for the hydrogenation of ketoisophorone and cinnamaldehyde, pointed out by DFT calculations that H_2 dissociation can occur on the Mn surface, with this process being the rate-determining step. However, the reaction rate significantly increases after impregnation with 5% Pt, by dissociation on Pt particles and spillover to the support. Regarding selectivity, they found that the adsorption of ketoisophorone on Pt was much weaker than on the supports, and as consequence, similar selectivity is achieved on OMS or Pt/OMS catalysts, producing selectively the C=C hydrogenation to levodione. In the case of cinnamaldehyde, hydrocinnamaldehyde or cinnamyl alcohol is produced on OMS or Pt/OMS, respectively, because in the last case, cinnamaldehyde is adsorbed mainly on Pt surface. In this sense, in our case, the adsorption of citral on the Pt surface can be also favored after H_2 pretreatment regarding the He one, taking into account the different electronic density of each type of Pt particles pointed out by the different BE values determined by XPS, as previously commented.

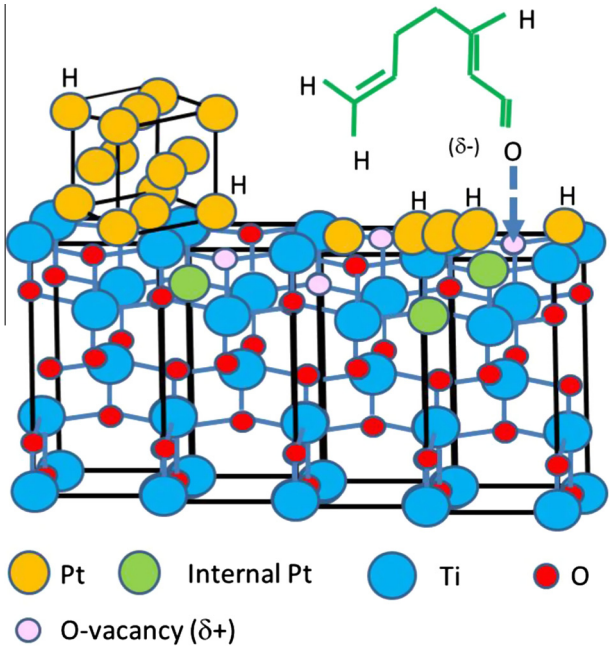

Fig. 8. Schematic representation of the Pt/TiO_2 structure and the interaction with the citral molecule.

Recently, it was also suggested that in the presence of citronellal, the adsorption mode of citral molecules changes [50]. Thus, in the absence of citronellal, citral is adsorbed through both C=C and C=O bonds, while in the presence of citronellal, a selective adsorption is carried out by the C=O bond, favoring the S_{UA}. In our case, this fact can be also significant, mainly in the case of He pretreated samples where citronellal is initially the main product formed (Fig. 2b). However, citronellal seems to be quickly hydrogenated to citronellol in these experimental conditions (Fig. 2b) probably favored by a stronger adsorption than UA. Moreover, while in the case of H_2 or even $He + H_2$ pretreated catalysts, the S_{UA} practically remains constant even at high conversion values; this parameter strongly decays in the case of He pretreated one. The different evolution of the product distribution is clearly related with the different nature of the active sites generated after each treatment and the transformations undergoing during reactions.

Thus, we have also previously suggested that there are some changes in the catalysts surface that favor the formation of UA, probably, by deactivation of the most active sites that initially favors the C=C hydrogenation or even cracking reactions. Accordingly to the stronger variation in the product distribution (Fig. 2a), these surface changes should be especially noticeable in the case of He pretreated Pt/TiO_2 catalysts and could be related, as commented, to a preferential adsorption of citronellal. Typically, the site deactivation is accompanied by permanently adsorbed species forming some "carbon-like" deposits that cover and deactivate these active sites. In a previous manuscript, Sing and Vanice [51] and later Manikandan et al. [52] pointed out that the deactivation of Pt/catalysts used in the citral hydrogenation can be due to irreversibly chemisorbed CO formed by decomposition of citral molecules.

Trying to analyze the amount and nature of these deposits, we have studied the used catalysts by TG and FTIR analysis. These results are summarized in Fig. 9. TGs experiments (Fig. 9a) point out that the amount of deposits is greater after He pretreatment, probably related with the greater acidity and cracking degree

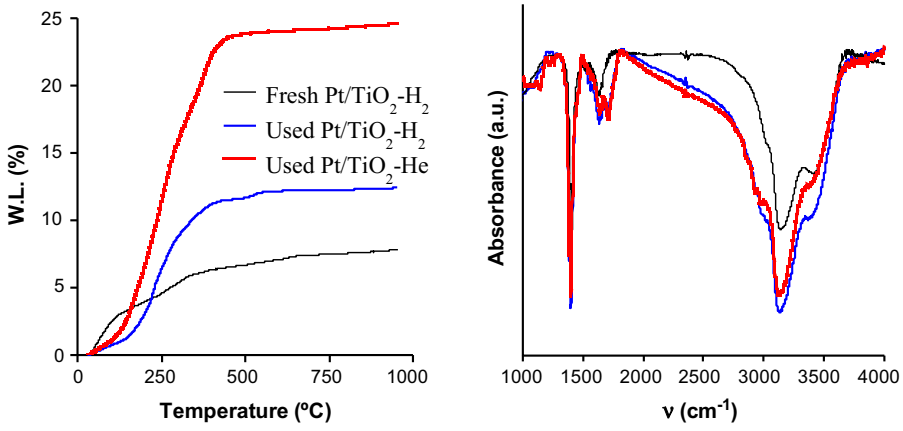

Fig. 9. Thermogravimetric (a) and FTIR analysis (b) of Pt/TiO_2 catalysts used in the citral hydrogenation after the corresponding pretreatment.

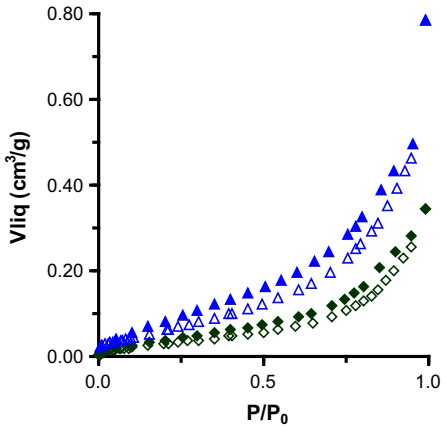

Fig. 10. N_2 adsorption isotherms of Pt/TiO_2 catalyst pretreated in H_2 before (▲) and after (♦) citral hydrogenation.

Table 6
Textural parameters of Pt/TiO_2 catalyst pretreated in H_2 before and after citral hydrogenation.

Catalyst	S_{BET}	W_0	L_0	V_{meso}	$V_{0.95}$
	$m^2\ g^{-1}$	$cm^3\ g^{-1}$	nm	$cm^3\ g^{-1}$	
Fresh Pt/TiO_2–H_2	111	0.045	1.62	0.397	0.442
Used Pt/TiO_2–H_2	62	0.024	2.59	0.232	0.256

observed in these experimental conditions. There are many references in the literature relating the catalysts performance with their acidity (mainly Brönsted acidity), coke formation, and catalysts deactivation. Although this fact was early pointed out some years ago by Topsøe et al. [53], there is even today a discussion matter and the deactivation by blocking acid sites is induced sometimes to increase the product selectivity [54,55]. Nevertheless, the nature of the deposits seems to be similar after both pretreatments. In both cases, the deposits are burned in the same temperature range, indicating a similar nature, which is confirmed also by the coincidence of the corresponding FTIR spectra (Fig. 9b). Only a new band appears together with those corresponding to the fresh catalysts, located at 1705 cm^{-1} which is assigned generally to C=O stretching vibration in carboxyl, ketones, and aldehydes groups [56]. This confirms the presence of oxygenated compounds adsorbed on the catalysts surface, which could block the acid sites of the catalysts avoiding cracking reactions and favoring the C=O hydrogenation. However, these results do not permit to elucidate when corresponding to adsorbed citral, citronellal, or other derivative intermediates.

These adsorbed materials are also partially blocking the porosity of the catalysts. As an example, in Fig. 10 are compared the N_2 adsorption isotherms of fresh and used catalysts (pretreated in H_2 flow). The corresponding textural parameters obtained in each case are summarized in Table 6. Results point out that the total pore volume ($V_{0.95}$) and the S_{BET} of catalysts practically decrease to the half. Nevertheless, the blockage of a specific porosity is not observed, but microporosity (W_0) and mesoporosity (V_{meso}) have decreased in the same proportion.

Taking into account the results and discussion provided, probably, both activity and selectivity can be improved by fitting the experimental conditions of treatment in H_2 (temperature and time) to balance as possible the positive effect TiO_2 reduction (concentration of vacancies) and the negative effect of Pt sintering and Pt diffusion into the TiO_2 structure, because internal Pt should be catalytically inactive. The use of thermal treatment under vacuum [36] or alternative reductants such as $NaBH_4$ [57] were also suggested to generate oxygen vacancies in TiO_2, and permit to obtain very high Pt dispersion regarding thermal treatments [58]. Moreover, the determination of the adsorption sites and their characteristics by additional experiments (spectroscopic studies, theoretical (DFT) calculations) confirming the observations analyzed here are also needed to control the activity and selectivity of hydrogenation catalysts.

4. Conclusions

The influence of pretreatment conditions of Pt/TiO_2 catalysts was analyzed by different techniques. The activity and selectivity to unsaturated alcohols are favored after H_2 pretreatments regarding the He ones in the same experimental conditions. This fact is related with a partial reduction of TiO_2 under H_2 flow that favors a strong metal–support interaction and the mobility of Pt species, avoiding the formation of three-dimensional Pt nanoparticles during pretreatment. Active and selective sites were ascribed to the synergetic effect of oxygen vacancies on the TiO_2 support and Pt metallic particles favoring the adsorption of citral through the C=O bond and a high availability of atomic hydrogen on highly dispersed Pt nanoparticles. However, if the decomposition of the precursor salt is carried out under He flow, a posterior H_2 treatment leads to an increase of selectivity but does not favor the catalytic activity.

The deposition of adsorbed oxygenated compounds during reaction takes place in a greater extent after pretreatment in He flow, probably related with the higher acidity and cracking activity detected in these experimental conditions. These adsorbed compounds block the more active sites also favoring the citral adsorption though the C=O bonds and the subsequent hydrogenation to unsaturated alcohols. Thus, high S_{UA} values are maintained at high conversion values after pretreatments in H_2 flow.

Acknowledgments

This research has been supported by the Spanish and FEDER projects CTM2010-18889 (MICINN), CTQ2013-44789-R (MINECO), and P12-RNM-2892 (Junta de Andalucía). E.B.G. also acknowledges for a predoctoral fellowship associated to the CTM2010-18889 project.

References

[1] H. Surburg, J. Panten, Common Fragrance and Flavor Materials: Preparation, Properties and Uses, WILEY-VCH, Weinheim, Germany, 2006.
[2] G.S. Clark, Geraniol, Perfumer & Flavorist 23 (1998) 19.
[3] W. Chen, A.M. Viljoen, S. Afr, J. Bot. 76 (2010) 643.
[4] P. Barbaro, F. Liguori, Heterogenized Homogeneous Catalysts for Fine Chemicals Production, Springer, London, 2010.
[5] E. Bailón-García, F.J. Maldonado-Hódar, A.F. Pérez-Cadenas, F. Carrasco-Marín, Catalysts 3 (2013) 853.
[6] E. Asedegbega-Nieto, A. Guerrero-Ruiz, I. Rodriguez-Ramos, Carbon 44 (2006) 804.
[7] G. Borda, H. Rojas, J. Murcia, J.L.G. Fierro, P. Reyes, M. Oportus, React. Kinet. Catal. Lett. 92 (2007) 369.
[8] I.M.J. Vilella, S.R. Miguel, C.S.-M.d.L. Lecea, Á. Linares-Solano, O.A. Scelza, Appl. Catal. A: Gen. 281 (2005) 247.
[9] A. Giroir-Fendler, D. Richard, P. Gallezot, Stud. Surf. Sci. Catal. 41 (1988) 171.
[10] U.K. Singh, M.A. Vannice, J. Catal. 199 (2001) 73.
[11] S.A. Ananthan, V. Narayanan, in: Proceedings of the International Conference on Nanoscience, Engineering and Technology, ICONSET, 2011, vol. 23.
[12] S.A. Ananthan, N. Vengidusamy, K. Giribabu, R. Suresh, Adv. Mater. Res. 584 (2012) 229.
[13] S.J. Tauster, S.C. Fung, J. Catal. 55 (1978) 29.
[14] T. Ekou, L. Ekou, A. Vicente, G. Lafaye, S. Pronier, C. Especel, P. Marecot, J. Mol. Catal. A: Chem. 337 (2011) 82.
[15] G. Lafaye, T. Ekou, C. Micheaud-Especel, C. Montassier, P. Marecot, Appl. Catal. A: Gen. 257 (2004) 107.
[16] M. Bidaoui, C. Especel, N. Bouchenafa-Saib, D. Duprez, O. Mohammedi, S. Royer, Appl. Catal. A: Gen. 445–446 (2012) 14.

[17] S. Brunauer, P.H. Emmett, E. Teller, J. Am. Chem. Soc. 60 (1938) 309.
[18] M.M. Dubinin, Carbon 23 (1985) 373.
[19] MM. Dubinin, Russ. J. Phys. Chem. 39 (1965) 1305.
[20] F. Stoeckli, Porosity in Carbons – Characterization and Applications, Arnold, London, 1995.
[21] J.F. Vivo-Vilches, E. Bailón-García, A.F. Pérez-Cadenas, F. Carrasco-Marín, F.J. Maldonado-Hódar, Carbon 68 (2014) 520.
[22] J.E. Benson, M. Boudart, J. Catal. 4 (1965) 704.
[23] G.R. Wilson, W.K. Hall, J. Catal. 17 (1970) 190.
[24] A.R. González-Elipe, A. Fernández, J.P. Espinós, G. Munuera, J. Catal. 131 (1991) 51.
[25] M.E. Nagassa, A.E. Daw, W.G. Rowe, A. Carley, D.W. Thomas, R. Moseley, Clin. Oral Implan. Res. 19 (2008) 1317.
[26] A. Orendorz, J. Wüsten, C. Ziegler, H. Gnaser, Appl. Surf. Sci. 252 (2005) 85.
[27] A. Samokhvalov, E.C. Duin, S. Nair, B.J. Tatarchuk, Surf. Interface Anal. 42 (2010) 1476.
[28] C.A. Leon, J.M. Solar, V. Calemma, L.R. Radovic, Carbon 30 (1992) 797.
[29] E. Bailón-García, F. Carrasco-Marín, A.F. Pérez-Cadenas, F.J. Maldonado-Hódar, Appl. Catal. A: Gen. 482 (2014) 318.
[30] J. Alvarez-Rodríguez, I. Rodríguez-Ramos, A. Guerrero-Ruiz, E. Gallegos-Suarez, A. Arcoya, Chem. Eng. J. 204–205 (2012) 169.
[31] E. Bailón-García, F. Carrasco-Marín, A.F. Pérez-Cadenas, F.J. Maldonado-Hódar, Development of carbon xerogels as alternative Pt-supports for the selective hydrogenation of citral, Catal. Commun. 58 (2014) 64–69.
[32] S. Santiago-Pedro, V. Tamayo-Galván, T. Viveros-García, Catal. Today 213 (2013) 101.
[33] J.L. Dong, J.H. Zhu, Q.H. Xu, Appl. Catal. A: Gen. 112 (1994) 105.
[34] F.J. Maldonado-Hódar, C. Moreno-Castilla, A.F. Pérez-Cadenas, Appl. Catal. B: Environ. 54 (2004) 217.
[35] M.D. Hernández-Alonso, A.R. Almeida, J.A. Moulijn, G. Mul, Catal. Today 143 (2009) 326.
[36] M. Xing, J. Zhang, F. Chen, B. Tian, Chem. Commun. 47 (2011) 4947.
[37] P. Gallezot, D. Richard, Catal. Rev. 40 (1998) 81.
[38] M. Steffan, F. Klasovsky, J. Arras, C. Roth, J. Radnik, H. Hofmeister, P. Claus, Adv. Synth. Catal. 350 (2008) 1337.
[39] S.D. Jackson, M.B.T. Keegan, G.D. Mclellan, P.A. Meheux, G. Webb, R.B. Moyes, P.B. Wells, R. Whyman, J. Willis, Preparation and Properties of a Pt/Silica and its Comparison with Europt-1, in: G. Poncelet (Ed.), Studies in Surface Science and Catalysis, Preparation of Catalysts V Scientific Bases for the Preparation of Heterogeneous Catalysts Proceedings of the Fifth International Symposium, Elsevier, Amsterdam, 1991, pp. 135–144.
[40] O.K. Ezekoye, A.R. Drews, H.W. Jen, R.J. Kudla, R.W. McCabe, M. Sharma, J.Y. Howe, L.F. Allard, G.W. Graham, X.Q. Pan, J. Catal. 280 (2011) 125.
[41] P. Claus, Top. Catal. 5 (1998) 51.
[42] F. Delbecq, P. Sautet, J. Catal. 152 (1995) 217.
[43] A. Giroir-Fendler, D. Richard, P. Gallezot, Catal. Lett. 5 (1990) 175.
[44] J.C. Conesa, P. Malet, G. Munuera, J. Sanz, J. Soria, J. Phys. Chem. 88 (1984) 2986.
[45] A.R. Gonzalez-Elipe, P. Malet, J.P. Espinos, A. Caballero, G. Munuera, Stud. Surf. Sci. Catal. 48 (1989) 427.
[46] M.G. Sanchez, J.L. Gazquez, J. Catal. 104 (1987) 120.
[47] J.P. Stassi, P.D. Zgolicz, V.I. Rodríguez, S.R. de Miguel, O.A. Scelza, Appl. Catal. A: Gen. 497 (2015) 58.
[48] M. Bidaoui, C. Especel, S. Sabour, L. Benatallah, N. Saib-Bouchenafa, S. Royer, O. Mohammedi, J. Mol. Catal. A: Chem. 399 (2015) 97.
[49] H.G. Manyar, B. Yang, H. Daly, H. Moor, S. McMonagle, Y. Tao, G.D. Yadav, A. Goguet, P. Hu, C. Hardacre, ChemCatChem 5 (2013) 506.
[50] H. Daly, H.G. Manyar, R. Morgan, J.M. Thompson, J.J. Delgado, R. Burch, C. Hardacre, ACS Catal. 4 (2014) 2470.
[51] U.K. Singh, M. Albert Vannice, J. Catal. 191 (2000) 165.
[52] D. Manikandan, D. Divakar, T. Sivakumar, Catal. Lett. 123 (2008) 107.
[53] N.Y. Topsøe, K. Pedersen, E.G. Derouane, J. Catal. 70 (1981) 41.
[54] V.G. Komvokis, S. Karakoulia, E.F. Iliopoulou, M.C. Papapetrou, I.A. Vasalos, A.A. Lappas, K.S. Triantafyllidis, Catal. Today 196 (2012) 42.
[55] S. Müller, Y. Liu, M. Vishnuvarthan, X. Sun, A.C. van Veen, G.L. Haller, M. Sanchez-Sanchez, J.A. Lercher, J. Catal. 325 (2015) 48.
[56] C. Moreno-Castilla, F. Carrasco-Marín, F.J. Maldonado-Hódar, J. Rivera-Utrilla, Carbon 36 (1998) 145.
[57] W. Fang, M. Xing, J. Zhang, Appl. Catal. B: Environ. 160–161 (2014) 240.
[58] J.L. Figueiredo, M.F.R. Pereira, P. Serp, P. Kalck, P.V. Samant, J.B. Fernandes, Carbon 44 (2006) 2516.